
The Dependence of Galaxy Properties on the Underlying 3D Matter Density Field at $2.0 < z < 2.5$

Rieko MOMOSE^{1,2,3,4}, Khee-Gan LEE³, Metin ATA^{7,3}, Benjamin HOROWITZ^{5,6}
and Jeyhan S. KARTALTEPE⁸

¹Observatories of the Carnegie Institution for Science, 813 Santa Barbara Street, Pasadena, CA 91101, USA

²Department of Astronomy, School of Science, The University of Tokyo, 7-3-1 Hongo, Bunkyo-ku, Tokyo, 113-0033, Japan

³Kavli Institute for the Physics and Mathematics of the Universe (WPI), UTIAS, The University of Tokyo, Kashiwa, Chiba 277-8583, Japan

⁴The Institute for AI and Beyond, The University of Tokyo, Tokyo 113-8655, Japan

⁷The Oskar Klein Centre, Department of Physics, Stockholm University, AlbaNova University Centre, SE 106 91 Stockholm, Sweden

⁵Department of Astrophysical Sciences, Princeton University, Princeton, NJ 08544, USA

⁶Lawrence Berkeley National Laboratory, 1 Cyclotron Road, Berkeley, CA 94720, USA

⁸Laboratory for Multiwavelength Astrophysics, School of Physics and Astronomy, Rochester Institute of Technology, 84 Lomb Memorial Drive, Rochester, NY 14623, USA

*E-mail: rmomose@carnegiescience.edu

Received (reception date); Accepted (acceptation date)

Abstract

We study the environmental effect of galaxy evolution as a function of the underlying 3D dark matter density for the first time at $z = 2 - 2.5$, in which the underlying matter density is reconstructed from observed galaxies through dynamical forward modeling techniques. Utilizing this map, we investigate the dependence of the star formation activities and galaxy types (mergers, submillimeter galaxies, active galactic nuclei, and quiescent galaxies) on the matter overdensity Δ_{local} and stellar mass. For the first time, we are able to probe underdense regions ($\Delta_{\text{local}} < 1$) in addition to overdensities. We find that star formation activity generally depends on the stellar mass, not the matter density. We also find evidence that: (1) an absence of mergers and submillimeter galaxies in higher-density regions but otherwise no trend across lower-density bins, (2) the increase of active galactic nuclei and quiescent galaxy prevalence as a function of matter density, and (3) the increase of all aforementioned categories with the stellar mass. These results indicate that stellar mass is the main driver of galaxy evolution at the cosmic noon. Our novel approach directly using reconstructed dark matter density maps demonstrates the new capability of the environmental effect studies in galaxy evolution at higher redshift.

Key words: galaxies: evolution — galaxies: star formation — large-scale structure of universe

1 Introduction

The understanding of galaxy formation and evolution has accelerated for over the last decades thanks to numerous

galaxy observations from local to the high- z universe. One of the notable findings is the bimodality of galaxy populations in color–magnitude or color–star formation rate (SFR) / specific SFR (sSFR) diagrams in the local to

as far as redshift $z \sim 3$ universe (e.g., Strateva et al. 2001; Kauffmann et al. 2003; Blanton et al. 2003; Blanton et al. 2005; Baldry et al. 2004; Willmer et al. 2006; Wyder et al. 2007; Williams et al. 2009; Blanton & Moustakas 2009; Brammer et al. 2009; Wetzelet al. 2012). Previous studies have found two distinct galaxy populations within the bimodality. One is referred to as the blue cloud consisting of star-forming galaxies, and the other is the red sequence of early-type galaxies with low or absence of new star formation. This galaxy bimodality is interpreted as the consequence of a change in two galaxy populations transitioning from the blue star-forming to the red quiescent over time. In other words, star-forming galaxies transform their physical properties, such as shape, color, and stellar ages, while quenching their star formation. Understanding the physical origin or processes that halt star formation and transit from the star-forming to quiescent phase in galaxies is therefore fundamental to unveiling galaxy formation and evolution.

Although several physical mechanisms for quenching star formation in galaxies have been proposed in the literature, they can generally be categorized as “internal” and “external processes” (e.g., Peng et al. 2010). The “internal process” or “mass quenching” includes any processes operating in individual galaxies themselves that link to or depend on the galaxy mass, such as feedback from active galactic nuclei (AGN) from the central supermassive black hole (SMBH) (e.g., Croton et al. 2006; Fabian 2012; Fang et al. 2013; Ito et al. 2022), supernova explosions, and stellar wind (e.g., Dekel & Silk 1986; Dalla Vecchia & Schaye 2008). Those processes can scatter out or heat the cold, dense gas available for forming stars, eventually obstructing the cycle of next star formation.

The second is an “external process,” also dubbed “environmental quenching.” This includes all physical processes originating from environments around galaxies leading to quench the star formation and work more effectively in higher density environments, such as galaxy groups, subclusters, and clusters. A variety of physical processes has been proposed in the literature. Galaxy interactions and mergers are considered to enhance star formation while simultaneously increasing the mass of the central SMBHs that, eventually, bring on the quenching of star formation (e.g., Sanders & Mirabel 1996; Springel et al. 2005; Springel et al. 2005; Hopkins et al. 2006; Hopkins et al. 2008; Yuan et al. 2010; Alexander & Hickox 2012). Likewise, high-speed fly-by galaxy encounters within clusters and subclusters, known as galaxy harassment, can eventually lead to the quenching while causing morphological transformations and starbursts (e.g., Moore et al. 1996; Moore et al. 1998; Smith et al. 2010; Smith

et al. 2013; Smith et al. 2015). The removal of gas in the interstellar regions by ram pressure stripping and tidal stripping in clusters or subclusters results in strangulation, which starves the galaxy and subsequently quenches the future star formation (e.g., Gunn & Gott 1972; Toomre & Toomre 1972; Larson et al. 1980; Balogh et al. 2000; Kawata & Mulchaey 2008; McCarthy et al. 2008; Bekki 2014; Smith et al. 2016; Boselli et al. 2022).

The dominant process for inducing galaxy quenching, either mass or environmental, is still hotly debated, though evidence indicates both processes contribute. It is commonly believed that at lower redshifts ($z < 1$), mass quenching seems to be dominant in high mass or central galaxies, whereas the environmental quenching becomes more important in low mass or satellite galaxies (e.g., Peng et al. 2010; Peng et al. 2012; Sobral et al. 2011). This trend seems to change in the earlier universe, but the evidence is still inconclusive. Darvish et al. 2016 have studied the effect of mass and environment on galaxy properties up to $z = 3$ using photometric redshift samples, and suggested that mass quenching plays a dominant role at $z > 1$ and the environmental quenching is relevant only at $z < 1$. Several other studies have also reported similar results (e.g., Muzzin et al. 2012; Nantais et al. 2016) at $z \sim 1 - 1.5$. However, environmental quenching has been observed up to $z = 2 - 3$ in other works. (e.g., Fossati et al. 2017; Guo et al. 2017; Kawinwanichakij et al. 2017; Ji et al. 2018; Zavala et al. 2019; Chartab et al. 2020; Ando et al. 2020). Further studies on the environmental effects of galaxy formation and evolution are necessary for deeper insight into the quenching mechanisms at higher redshift beyond $z \geq 1$.

One of the common challenges in studies of the environmental effects is correctly estimating the environment or overdensity around galaxies. They are generally assessed by galaxy distributions, often based on photometric redshifts, using different estimators, such as N -th nearest neighbors, Friends-of-Friends grouping algorithm, counts-in-cylinders, and adaptive weighted kernel smoothing. However, evaluating galaxy overdensities at higher redshift ($z > 2$) poses significant challenges. Firstly, the larger uncertainties of photo- z estimates at higher redshift reduce the contrast of dark matter density over tens of Megaparsecs along the line of sight. This effect gives a smaller value to galaxy overdensities than the real ones. Secondly, an estimated galaxy environment could be biased toward regions where higher mass galaxies mainly reside because the stellar-mass completeness limit of a survey increases with redshift. Thirdly, recent observations have shown that galaxy distributions cannot always trace the underlying matter density when a particular type of

galaxy is used such as Ly α emitters (e.g., Overzier et al. 2008; Toshikawa et al. 2016; Shimakawa et al. 2017; Shi et al. 2019; Liang et al. 2021; Momose et al. 2021b; Momose et al. 2021a; Ito et al. 2021; Huang et al. 2022). One might derive incorrect overdensities if we use that type of galaxies to evaluate the environment. Fourthly, with many traditional environmental measures such as N -th nearest neighbors and counts-in-cylinders, it is difficult to correct for the observational selection functions even with spectroscopic data. Those reasons lead us to consider another methodology for evaluating the environments around galaxies at higher redshift.

In this study, we estimate the galaxy environments based on the underlying 3D dark matter density. Our novel approach corrects for the issues mentioned above, that could arise from evaluating the dark matter distribution based on a density field derived from the spatial distribution of galaxies. Theoretical work over the past decade has led to some novel computational techniques to reconstruct the underlying 3D matter density within a survey volume using spectroscopic galaxy positions as tracers (e.g., Jasche & Wandelt 2013; Kitaura et al. 2021; Horowitz et al. 2019; Horowitz et al. 2021; Ata et al. 2021; Ata et al. 2022). Those reconstructed density fields have advantages in identifying the matter density accurately and are superior to studies referring to galaxy distributions alone because they have corrected for galaxy bias, survey selection functions, and redshift space distortions. We utilize such reconstructed matter density fields as a proxy of the environments in order to investigate the dependence of star formation activities and galaxy types on the mass and environments of galaxies at $z \sim 2$. This allows us to address the dominant physical mechanisms for quenching star formation in galaxies.

This study investigates correlations between the matter density and galaxy properties, specifically, star formation activities and the fraction of submillimeter galaxies, mergers, quiescent galaxies, and AGN. The layout of this paper is as follows. We introduce the data and method used in this study in Section 2 and show our results in Section 3. Discussions about the galaxy evolution based on our results are presented in Section 4.

2 Data

2.1 Matter Density Maps

This study uses a reconstructed 3D matter density field, named the COntained Simulations of The COsmos field (COSTCO, Ata et al. 2022), to evaluate the local matter density around galaxies in the Cosmic Evolution Survey

field (COSMOS; Capak et al. 2007; Scoville et al. 2007). Although the detail of the methodology is fully described in Ata et al. (2022), we provide its summary below.

The COSTCO is a suite of constrained simulations designed to resemble three-dimensional galaxy distributions in the COSMOS field at $2.0 \leq z \leq 2.52$. Firstly, a binned galaxy density field was calculated from a compilation of galaxy spectroscopic surveys: zCOSMOS-Deep (Lilly et al. 2007), VUDS (Le Fèvre et al. 2015), MOSDEF (Kriek et al. 2015), and ZFIRE (Nanayakkara et al. 2016), with the respective angular and radial selections carefully accounted for (Ata et al. 2021). Using the COSMIC BIRTH algorithm, a nested Bayesian inference algorithm (Kitaura et al. 2021; Ata et al. 2021), initial fluctuations (at $z=100$) were estimated such that will eventually evolve into a matter density field consistent with the observational galaxy field at $2.0 < z < 2.55$. A suite of cosmological N -body simulations were then performed from the posterior sample of these initial conditions in order to describe the evolution of observed structures over cosmic time, which is dubbed COSTCO. The COSTCO matter density field used in this study covers the central 0.9 deg^2 region of the COSMOS footprint where most of the spectroscopic data reside, spanning a redshift range of $z = 2 - 2.52$ and has a binning of $0.5 h^{-1} \text{ cMpc}$. Ata et al. (2022) have estimated the effective reconstruction scale of COSTCO to be approximately $\approx 4.5 h^{-1} \text{ cMpc}$.

Figure 1 demonstrates the normalized cumulative profile and number density of the matter density contrast or “overdensity”, $\Delta_{\text{pix}} \equiv \rho / \langle \rho \rangle$, in the entire COSTCO field. This Δ_{pix} is the output of reconstructions and one-pixel values. The COSTCO density field is occupied by the lowest densities ($0 \leq \Delta_{\text{pix}} < 2$) with more than 90% volume filling factor.

Instead of utilizing Δ_{pix} , we used the density contrast within $2 h^{-1} \text{ cMpc}$ in a radius (i.e., $4 h^{-1} \text{ cMpc}$ in a diameter) around individual galaxies as their local environment, which refers to Δ_{local} , in the following analysis. We choose the scale since [a] the smoothed simulation of $4 h^{-1} \text{ cMpc}$ still showed good agreements on the mean power spectrum of the COSTCO field (see Supplementary Fig. 5 in Ata et al. 2022) and [b] the sample size on the matter density subsamples introduced in Section 2.2 does not vary by $4 h^{-1} \text{ cMpc}$ or $4.5 h^{-1} \text{ cMpc}$.

2.2 Galaxy Sample

In this study, we used several spectroscopic catalogs targeting $2.0 \leq z \leq 2.55$ galaxies and constructed a compiled catalog (Smolčić et al. 2012; Hashimoto et al. 2013; Nakajima et al. 2013; Shibuya et al. 2014; Le

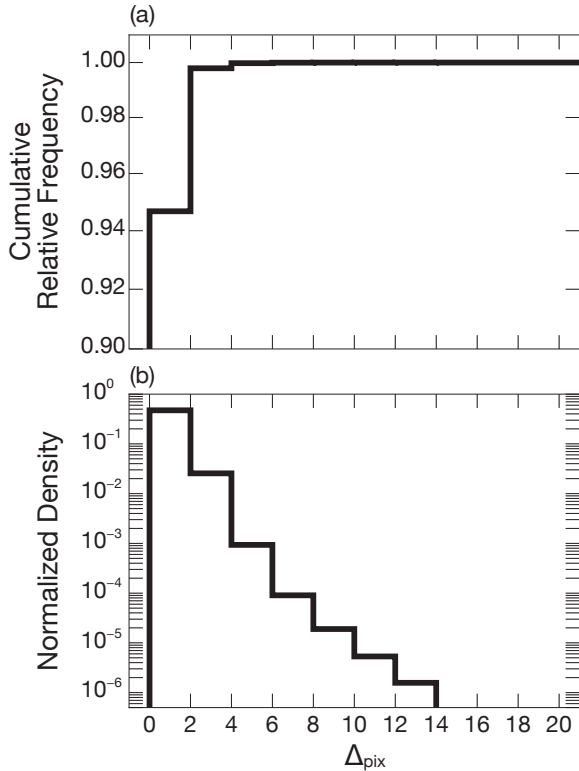


Fig. 1. (a) The normalized cumulative profile and (b) number density of the density contrast, Δ_{pix} , in the COSTCO field.

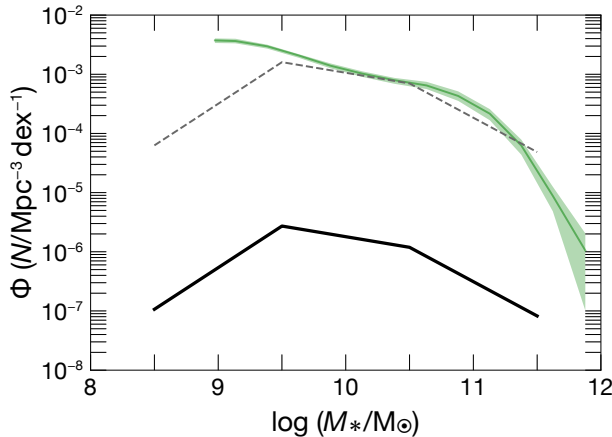


Fig. 2. The stellar mass function of our mass-complete sample (black straight line) and photo- z galaxies at $2.0 \leq z \leq 2.5$ in Weaver et al. (2023) (green line). The dashed line is the mass-complete sample with offsets for shape comparison with the one by Weaver et al. (2023).

Fèvre et al. 2015; Kriek et al. 2015; Nanayakkara et al. 2016; Lee et al. 2016; Lee et al. 2018; Brisbin et al. 2017; Michałowski et al. 2017; Champagne et al. 2021; Lilly et al. in prep). First, we extracted galaxies at $2.0 \leq z \leq 2.55$ laying within the COSMOS field. Then, we applied quality cuts defined in each catalog and cross-matched each other with a maximum allowable separation of $0''.5$. The final compiled catalog contains 1784 galaxies,

Table 1. The Number of Galaxies Used in This Study

	(1)	(2)	(3)
All	1344	(1223, 121)	
Lowest- Δ ($\Delta_{\text{local}} < 1$)	519	(484, 35)	
Low- Δ ($1 \leq \Delta_{\text{local}} < 2$)	653	(588, 65)	
Intermediate- Δ ($2 \leq \Delta_{\text{local}} < 4$)	154	(135, 19)	
High- Δ ($\Delta_{\text{local}} \geq 4$)	18	(16, 2)	
Mergers [†]	19	(9, 10)	
SMGs	11	(1, 10)	
AGNs	23	(4, 19)	
QGs	12	(2, 10)	

The number of the mass-completeness sample in the COSTCO field. (1) Category of subsamples. (2) Total number of galaxies in each subsample. (3) Number of low- and high-mass galaxies in a subsample. This study regards galaxies with $M_* < 10^{10.5} M_{\odot}$ as low-mass and with $M_* \geq 10^{10.5} M_{\odot}$ as high-mass, respectively. Their numbers are denoted in the table as (low-mass galaxies, high-mass galaxies).

[†] We list the number of individual merging galaxies instead of the one of merging pairs

which are referred to as the “full sample”.

The stellar mass (M_*), SFR , and $sSFR$ of galaxies in the compiled catalog were taken from the latest photo- z catalog, COSMOS2020 (Weaver et al. 2022). In this study, we use the above quantities using estimates derived from spectral energy distribution (SED) fitting code, *LePhare* (Ilbert et al. 2006), in *FARMER* catalog of the COSMOS2020. We first cross-matched the compiled spectroscopic catalog with the COSMOS2020 within a $1.0''$ radius and obtained 1428 galaxies. We further applied the mass completeness criteria defined in the COSMOS2020¹,

$$\frac{M_{\text{lim}}(z)}{M_{\odot}} = -1.51 \times 10^6 (1+z) + 6.81 \times 10^7 (1+z)^2 \quad (1)$$

where M_{lim} is a redshift-dependent threshold in stellar mass (M_{\odot}). That results in 1344 complete mass samples for the COSTCO field. Galaxies above the mass completeness criteria are denoted as “mass-complete sample”, which we used in this study.

Galaxies targeted for spectroscopic observations are generally selected from photometric surveys, implying that they are just a subset of the galaxies within the photometry catalogs. Here, we compare M_* and SFR of our mass-complete sample and parent photometric catalog of COSMOS2020 in order to briefly examine if we can regard our galaxy samples as a representative of the COSMOS2020 in terms of their physical properties. In Figure 2, we compare the stellar mass function (SMF) of the mass-completeness sample in this study to the parent photometric catalog of COSMOS2020 (Weaver et al. 2023). The black line shows our SMF, whereas the dashed

¹ This equation is the same as one in Sec.6.2 of Weaver et al. 2022.

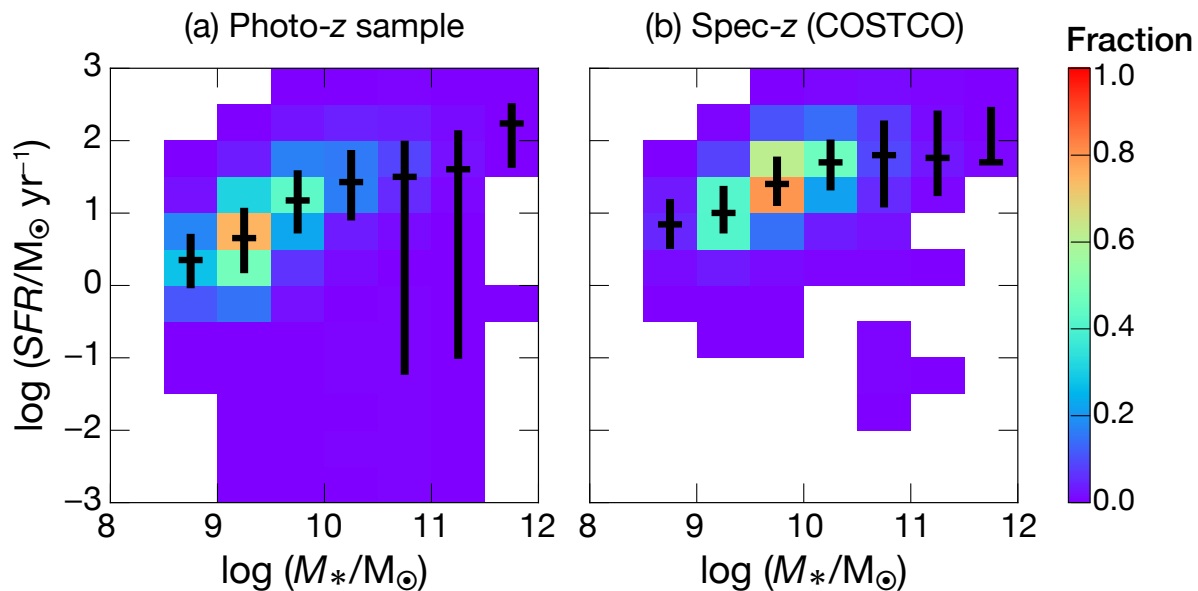


Fig. 3. The heatmap of galaxies in the main sequence diagram of (a) the COSMOS2020 at $1.9 \leq z \leq 2.6$ and (b) mass-completeness sample in the COSTCO field. The number of galaxies in each bin is normalized. A pixel with 0 is denoted by white. The median of each M_* pixel and the percentil 16th and 84th of SFR is plotted by plus marks.

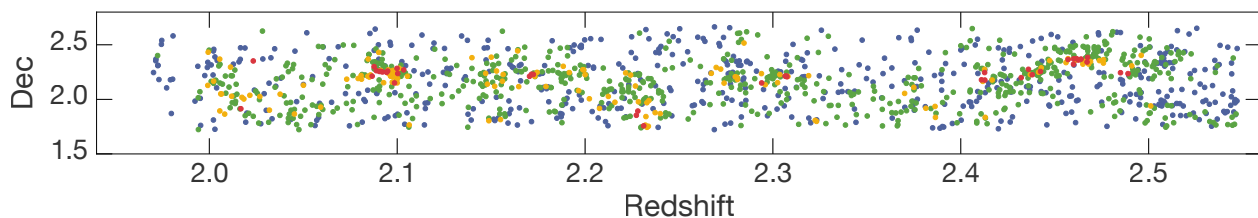


Fig. 4. Distributions of our galaxy samples in the COSTCO field in the Dec- z_{spec} plane. Color is based on the matter density subsamples – blue, green, yellow, and red indicate subsamples in $\Delta_{\text{local}} < 1$, $1 \leq \Delta_{\text{local}} < 2$, $2 \leq \Delta_{\text{local}} < 4$, and $\Delta_{\text{local}} \geq 4$.

line represents the normalized ones at $M_* = 10^{10} M_\odot$ for its shape comparison purposes. Note that we do not evaluate uncertainty for our SMF because we focus on its shape comparison. Besides, the bin size is larger than the one in Weaver et al. (2023) due to our limited sample size. We apply the bin size of $M_* = 10^1 M_\odot$ from $M_* = 10^8$ to $10^{12} M_\odot$ which is also used in our investigations shown in Section 3.2. Overall, our SMF has a smaller galaxy number density $\Phi(M_*)$ by 3–4 orders of magnitudes than the parent photo- z sample. The normalized SMF shown by the dashed line appears to have a consistent shape to the parent SMF of Weaver et al. (2023) at $M_* > 10^9 M_\odot$ within the uncertainties, despite the coarseness of our stellar mass bin. We also compare the 2D distribution (heatmap) of galaxies in the star formation main sequence diagram of COSMOS2020 and this study Figure 3. The heatmap for COSTCO shows the lack of galaxies with a lower SFR overall M_* range compared to samples in COSMOS2020. Besides, the peaks of both M_* and SFR in our samples are shifted to 0.5 dex higher values than the COSMOS2020

samples. Nonetheless, the median values of parent samples and ours are within the uncertainties. To sum up the comparison between parent COSMOS2020 samples and ours, our galaxies can be regarded as a proxy of their stellar mass, at least $M_* \geq 10^9 M_\odot$ under the coarse M_* bin. We also anticipate that the SFR values should be consistent within the error, at least in each M_* bin.

2.2.1 Subsamples

For this study, we construct three different subsamples to establish the link between galaxy evolution and environment or mass. The first is mass subsamples, which are used to examine the dependence on the density contrast. We divide our samples into two, low-mass and high-mass, according to their stellar masses. We define the threshold for the high-mass at $M_* = 10^{10.5} M_\odot$. We adopt this threshold because $M_* = 10^{10.5} M_\odot$ corresponds to the stellar mass reaching the peak of the stellar-to-halo mass relation and could be boundary mass resulting in a significant difference in the star formation history and subsequent quenching

(e.g., Moster et al. 2013; Behroozi et al. 2013; Behroozi et al. 2019). Note that you can find the impact of the threshold mass on the results in Appendix 1. The number of galaxies classified as either low-mass or high-mass is listed in Table 1. The fraction of high-mass galaxies is about 10% of the total in the COSTCO volume.

The second is the matter density subsamples to investigate mass dependence. Our mass-complete samples are divided into four density bins based on their Δ_{local} , where the underdense ($\Delta_{\text{local}} < 1$), low- ($1 \leq \Delta_{\text{local}} < 2$), intermediate- ($2 \leq \Delta_{\text{local}} < 4$), and high-density contrasts ($\Delta_{\text{local}} \geq 4$). The highest-densities of $\Delta_{\text{local}} \geq 4$ typically corresponds to the central regions of protoclusters (when compared with, e.g., Ata et al. 2022), while $2 \leq \Delta_{\text{local}} < 4$ are associated with protocluster outskirts. Galaxies residing in $1 \leq \Delta_{\text{local}} < 2$ regions, meanwhile, can be roughly regarded as ‘field’ galaxies. Finally, $\Delta_{\text{local}} < 1$ are in underdensities, although we have not made a careful comparison with the cosmic void catalog of Krolewski et al. (2018). Figure 4 shows galaxy distributions of mass-complete samples in Dec- z_{spec} plane with color-coded in each matter density subsample. Some of the high-density subsample galaxies are found at about the same position as well-known galaxy protoclusters – one is found at $z \sim 2.1$, and the other is at $z \sim 2.44$. It is also worth discussing the volume fraction of each matter density subsample relative to the entire volume and the density of galaxies in that density bin. We refer to a pixel value, Δ_{pix} , for this analysis. Each density subsample of $\Delta_{\text{pix}} < 1$, $1 \leq \Delta_{\text{pix}} < 2$, $2 \leq \Delta_{\text{pix}} < 4$, and $\Delta_{\text{pix}} \geq 4$ occupies 58.2, 36.5, 5.1, and 0.2% in the COSTCO volume. More than half of COSTCO volume is filled with underdense region on $\Delta_{\text{pix}} < 1$. Meanwhile, a number density of galaxies is $(2.8, 5.4, 9.6, 27.6) \times 10^{-6} \text{ cMpc}^{-3}$ in (lowest, low, intermediate, high)-density subsample. Given the mean number density for the entire COSTCO volume, $4.1 \times 10^{-6} \text{ cMpc}^{-3}$, a growth rate on a number density of galaxies with matter density is larger than the one expected from the change of matter density contrast. Note that this number density of galaxies does not vastly change when we even refer to Δ_{local} .

Finally, we also assess the dependence of quiescent galaxies (QGs), merging galaxies, submillimeter galaxies (SMGs) and AGN fractions on the density contrast. The QGs are identified with the same method proposed by Ilbert et al. (2013). They have classified QGs and star-forming galaxies based on the rest frame NUV, r , and J colors, such that QGs are defined with

$$m_{\text{NUV}} - m_r > 3(m_r - m_J) + 1 \quad \text{and} \quad m_{\text{NUV}} - m_r > 3.1 \quad (2)$$

Here, m_{NUV} , m_r , and m_J are the rest-frame NUV, r , and J magnitudes given in the COSMOS2020 catalog. We have

12 QGs in the COSTCO volume.

For the merging galaxies, SMGs, and AGNs, we performed a cross-match between the compiled catalog and several galaxy catalogs in the literature using a matching radius of $1.0''$. To find merging galaxies, we used two different merger catalogs from Silva et al. (2018) and Shah et al. (2020); details on the methodology of galaxy pairs identification can be found in the respective references. Although they have used different criteria for identifying galaxy pairs, both studies selected galaxies greater than $M_* > 10^{10} M_{\odot}$. We adopted the same threshold for our merger samples. As for SMGs, we refer to four catalogs (Smolčić et al. 2012; Brisbin et al. 2017; Michałowski et al. 2017; Champagne et al. 2021) and cross-matched them with our compiled spectroscopic catalog. For AGNs, we cross-matched with Straatman et al. (2016), Cowley et al. (2016) and Delvecchio et al. (2017). Cowley et al. (2016) have selected AGNs based on the rest frame radio, X-ray, or infrared luminosities. Delvecchio et al. (2017), meanwhile, have classified AGNs from 3 GHz radio sources using SED fitting, X-ray and mid-infrared diagnostics, and radio emission excess. The detailed criteria for AGN candidates is found in those studies. The numbers of mergers, SMGs, and AGNs used in this study are given in Table 1. Note for mergers that we count the number of individual merging galaxies, not each merging pair as one object. Because not all galaxies in merging pairs were cross-matched with the full sample, we got odd numbers.

3 Results

This section shows results to investigate two dependences of galaxy properties on local density environment, Δ_{local} , and stellar mass M_* .

3.1 Dependence On Matter Density Contrast

3.1.1 Global Trend

We demonstrate the actual number of galaxy samples to a certain density contrast in Figure 5-a. More than 80% of our samples are in underdense regions in $0 \leq \Delta_{\text{local}} < 2$. We also show the fraction of low-/high-mass galaxies at a given density contrast Δ_{local} in Figure 5-b. Qualitatively, the fraction of low-mass galaxies is always dominant over the full Δ_{local} range, whereas the fraction of high-mass galaxies gradually increases by about 20 – 30 % increasing the density contrast. However, those differences in the fraction of low- and high-mass galaxies as a function of the density contrast were statistically insignificant in the two-sample Kolmogorov–Smirnov test with p -value = 0.18. We note that the results on low-mass galaxies would not be

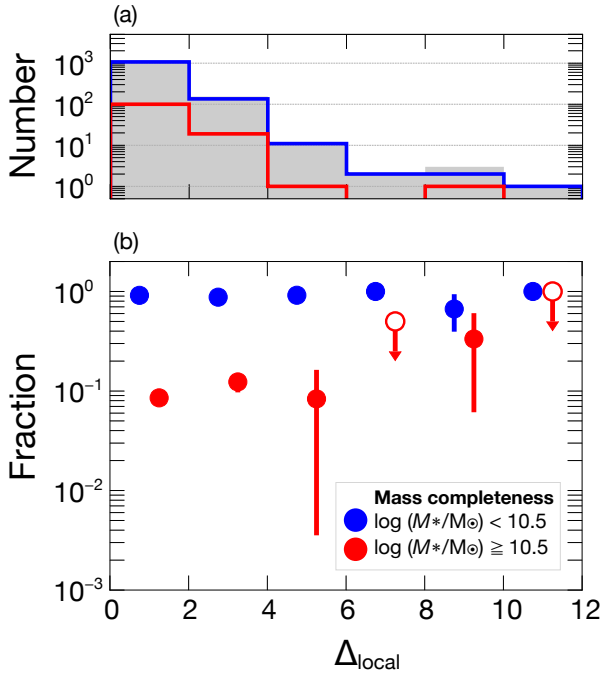


Fig. 5. (a) : Number histograms of galaxy samples as a function of the density contrast. (b): Fractions of low- and high-mass galaxies as a function of the density contrast. For both panels in (a) and (b), blue and red lines or markers represent low- and high-mass galaxy samples respectively. The upper limit of high-mass galaxies is also shown as white circles when none is found in a bin. We consider an estimate to be the upper limit, assuming one sample in a bin ($N_{\text{bin}} = 1$). These measurements are performed in each $\Delta_{\text{local}} = 2.0$ bin. The errors are calculated through a Poissonian approach as \sqrt{n}/N , where n and N are the numbers of targeting sample and total galaxies within an each Δ bin.

largely changed if we exclude galaxies with $M_* < 10^9 M_\odot$ since its fraction is small enough (3%).

3.1.2 Star Formation Activities

Figure 6 represents the median SFR and $sSFR$ as a function of density contrast. We should note that this study is the first to investigate galaxy trends in underdensities ($\Delta_{\text{local}} < 1$) beyond $z \gtrsim 1$.

The environmental trends for SFR is seen in Figure 6-a. We first find in low-mass galaxies that SFR is nearly constant about at $\log(SFR) = 1.3 - 1.4$ over the full Δ_{local} range. Note that although it has a factor of 4 difference between their lowest and highest values of SFR , it is still within the errors. The SFR of high-mass galaxies is also independent of the density contrast until $\Delta_{\text{local}} = 6$ within the error. In addition, we find that high-mass galaxies have possibly higher SFR by a factor of 2.5 – 3.1 than low-mass galaxies within this Δ_{local} range, though it is within an allowable error range. This implies that the SFR of both low- and high-mass galaxies do not depend on the density contrast up to some density level. Just as with the trend

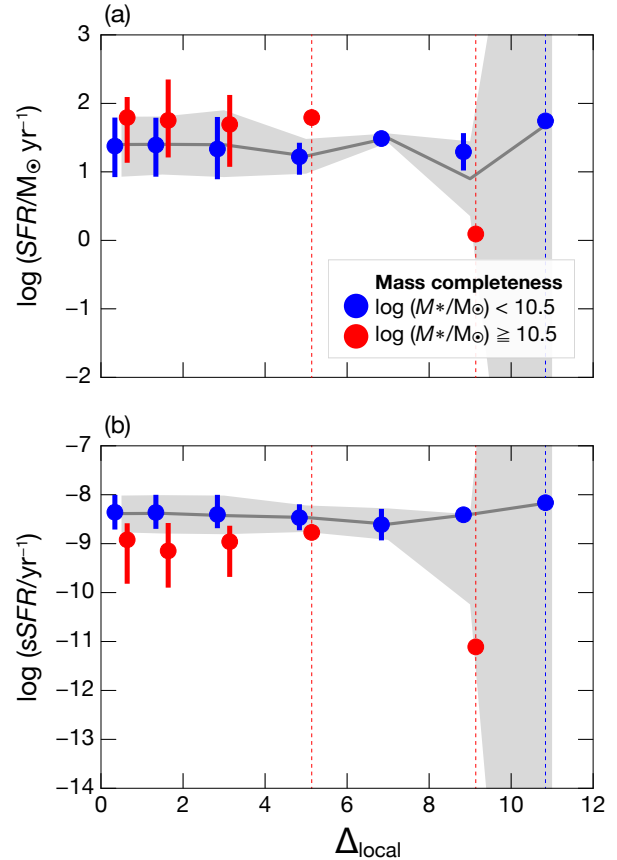


Fig. 6. The median (a) SFR and (b) $sSFR$ of low-/high-mass galaxies as a function of the density contrast. They are plotted in each $\Delta_{\text{local}} = 1.0$ at $\Delta_{\text{local}} < 2.0$ but each $\Delta_{\text{local}} = 2.0$ at $\Delta_{\text{local}} \geq 2.0$. The error bars indicate the percentiles 16th and 84th of SFR and $sSFR$. A gray line and shades are the medians and 68 percentiles of the entire mass-completeness sample. In the case of only one sample in a bin, we add an infinite error by dashed lines or grey shades because we cannot evaluate the 16th and 84th percentiles.

of SFR , the $sSFR$ shows little change over the wide Δ_{local} range in low-mass galaxies and at $\Delta_{\text{local}} < 6$ in high-mass galaxies (see in Figure 6-b).

Both SFR and $sSFR$ exhibit a rapid decline in median values on high-mass galaxies beyond $\Delta_{\text{local}} = 6$. Nonetheless, that may not be statistically significant due to substantial uncertainty caused by the small sample size ($N_{\text{bin}} = 1$). We will discuss more about it in Section 4.2.1.

3.1.3 Mergers, SMGs, AGNs, and QGs

Figure 7 demonstrates the fractions of galaxies that are mergers, SMGs, AGNs, and QGs as a function of the density contrast. We should caution that these samples are small due to limited availability of spec- z measurements on these classes. We have 19 mergers, 11 SMGs, 23 AGNs, and 12 QGs. Dividing these galaxy types into different masses yield even smaller subsamples. Details of their sample sizes are provided in Table 1.

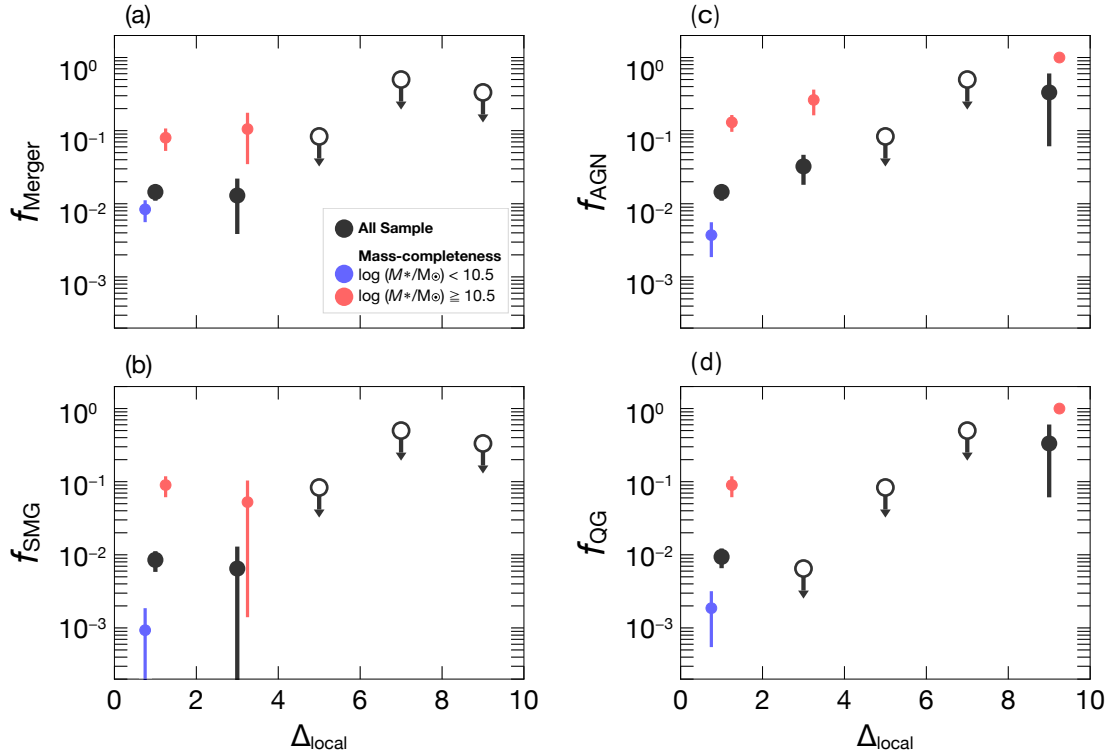


Fig. 7. The fraction of different galaxy types in each $\Delta_{\text{local}} = 2.0$ bin. Each sub panel demonstrates individual special galaxy type fractions of (a) mergers, (b) SMGs, (c) AGNs, and (d) QGs. Black, blue, and red circles represent fractions estimated from the mass-complete (i.e., all galaxies), low-, and high-mass galaxy samples. The errors are calculated through a Poissonian approach as \sqrt{n}/N , where n and N are the numbers of targeting galaxy type and total galaxies within an each Δ_{local} bin. The upper limit is also shown as white circles when no galaxy sample is found in a bin. We consider an estimate to be the upper limit, assuming one sample in a bin ($N_{\text{bin}} = 1$). Data points are slightly shifted horizontally for clarity.

Here we present four main results. First, we find an absence of mergers and SMGs in higher-density regions, particularly at $\Delta_{\text{local}} \geq 4$. Interestingly, this Δ_{local} range for the presence of mergers and SMGs, i.e., $\Delta_{\text{local}} = 0 - 4$, overlaps the Δ_{local} range, which shows a lack of dependence of SFR and $sSFR$ on the density contrast regardless of mass bin (see Section 3.1.2).

The second trend is the independence of mergers and SMGs fractions from the density contrast when we limit to the range where samples are found. The lack of fractional changes on the density is also apparent in the high-mass regime of both mergers and SMGs because more than half of those samples belong to the high-mass regime.

The third is the presence of AGNs and QGs in high-density environments at $\Delta_{\text{local}} \geq 4$. In addition, quite intriguingly, nearly all high-mass galaxies found in high density are either AGNs or QGs by showing f_{AGN} or $f_{\text{QG}} \sim 1$.

The fourth is the increase of AGNs and QGs fractions as a function of density contrast. The same increases are accentuated when the sample is limited to high-mass galax-

ies.

There are no observational works which we can directly compare our results for now because all past investigations in the fractions of mergers, QGs, SMGs, and AGN have been done based on the *galaxy* overdensity. Nonetheless, the comparison across studies would be helpful to obtain the deep insight into our results.

One of the frequently studied galaxy fraction is QG fraction. Likewise our results, some studies at lower redshifts have observed the increase of QG fractions with galaxy overdensities (e.g., Chuter et al. 2011; Quadri et al. 2012; Kawinwanichakij et al. 2017; Reeves et al. 2021). Kawinwanichakij et al. (2017) have evaluated the QG fraction at $0.5 < z < 2.0$ on the galaxy overdensity and observed the increase of the fraction. Reeves et al. (2021) have shown that QG fractions in $M_* > 10^{11} M_\odot$ at $1 < z < 1.5$ are systematically larger in their group samples than the field. In contrast, the opposite trend, i.e., an anti-correlation of QG fraction and galaxy overdensity, has been found in some studies (e.g., Tran et al. 2010; Lin et

al. 2016). A lack of dependence on galaxy overdensity has also been reported (e.g., Darvish et al. 2016). Therefore, a solid conclusion in QG fraction can not yet be arrived at, although our study is to our knowledge the first explicit analysis of environmental properties of QGs at $z > 2$.

The AGN fraction is also often examined in the literature. Many studies have suggested that AGN fraction depends on the galaxy environment at low-redshifts, in which the AGN fraction is found to be higher in underdense galaxy environments than overdense ones (e.g., Kauffmann et al. 2004; Silverman et al. 2009; von der Linden et al. 2010; Lopes et al. 2017). We should note that some studies have argued for no significant preference on galaxy overdensity for AGN fraction at the same low-redshift range (e.g., Miller et al. 2003; Man et al. 2019). In contrast, Lehmer et al. (2009) have detected a factor of 6.1 larger AGN fraction in the SSA22 protocluster at $z = 3.09$ than in the field. Similarly, the enhancements of AGN fractions have also been reported in protocluster or cluster environments at $z > 2$ (Digby-North et al. 2010; Polletta et al. 2021). This positive correlation between the AGN fraction and galaxy overdensities is clearly opposite to the one seen in low- z universe and could be more significant beyond $z = 2$ (Martini et al. 2013; Krishnan et al. 2017). Our results on the AGN fractions and its increase with density contrast Δ_{local} , would agree with this positive correlation found at higher redshift. However, a lack of AGN enhancement in an individual protocluster at $z \sim 2$ has been observed by Macuga et al. (2019), suggesting that there is still room for more discussion on the relation between the AGN fraction and the environment. Further work will be required to conclude that relationship.

Unlike AGN and QG fractions, the density dependence of mergers and SMG activity has not been well studied in the literature. The merger fraction in the $z > 2$ universe has generally been inconclusive. Some studies have observed a higher merger fraction in clusters than in fields (e.g., Lotz et al. 2013; Hine et al. 2016; Watson et al. 2019), while other studies have found no enhancement in clusters (e.g., Delahaye et al. 2017). The lack of enhancement or even the absence of mergers in the higher density regions in our data may be indicative of agreement with the latter studies or simply a result of the small sample size. We will discuss it in Sections 4.1 and 4.2.2. Many observations have reported that dusty star-forming galaxies represented by SMGs are often found in massive halos (e.g., Venemans et al. 2007; Hickox et al. 2012; Umehata et al. 2015; Wilkinson et al. 2017; Jones et al. 2017; Zeballos et al. 2018; Álvarez Crespo et al. 2021). In contrast, Miller et al. (2015) have claimed that SMGs at $z \leq 2.5$ are supposed to reside in less dense environments, not the most massive overdensities

from their semi-analytic simulations. Some observations have also drawn similar conclusions (e.g., Chapman et al. 2009; Casey 2016). Hence, the true relation between SMG prevalence and overdensity is still unclear.

3.2 Dependence On The Stellar Mass

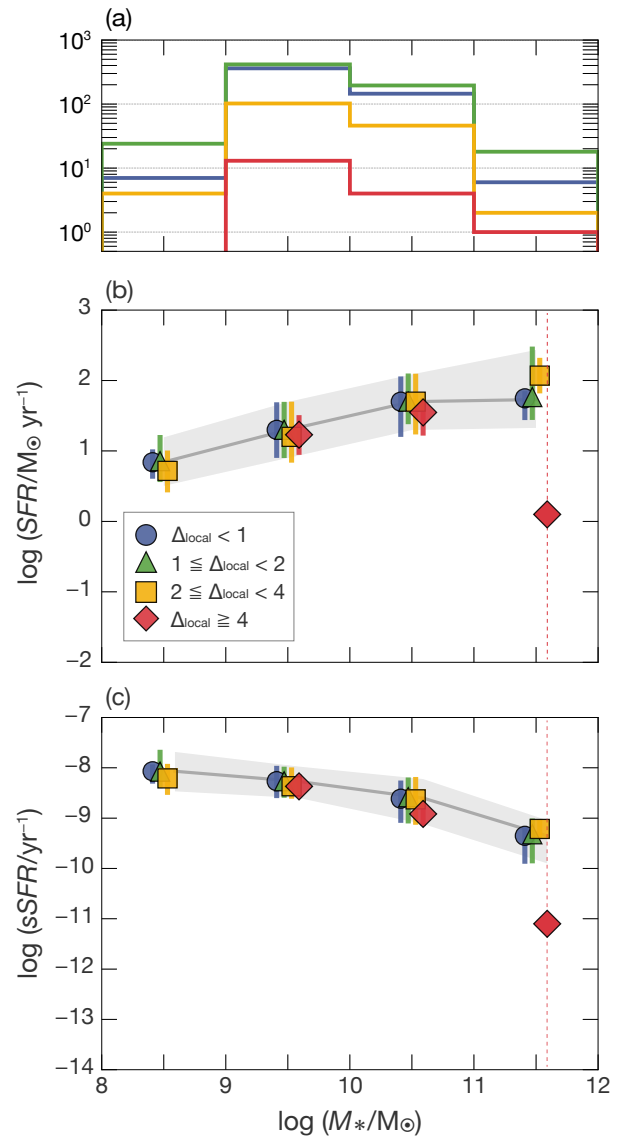


Fig. 8. (a) Number histograms of matter density subsamples in each $M_* = 10^1 M_\odot$ bin from $M_* = 10^8$ to $10^{12} M_\odot$. The median (b) SFR and (c) $sSFR$ to M_* in each $M_* = 10^1 M_\odot$ bin. For all panels, blue, green, yellow, and red indicate subsamples in $\Delta < 1$, $1 \leq \Delta < 2$, $2 \leq \Delta < 4$, and $\Delta \geq 4$. The error bars indicate the percentiles 16th and 84th of SFR and $sSFR$. A gray line and shades are the medians and 68 percentiles of SFR and $sSFR$ of the entire mass-completeness sample. Data points are slightly shifted horizontally for clarity. We give an infinite error bar to a data point at $M_* \geq 10^{10} M_\odot$ in $\Delta \geq 4$ subsample because there is only one sample in that bin.

Galactic properties are shaped and influenced by not only their environments but also their internal processes.

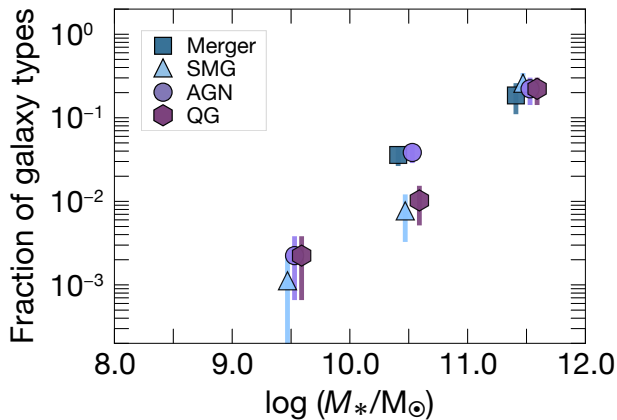


Fig. 9. The fraction of different special galaxy types in different logarithmic M_* bins from 10^8 to $10^{12} M_\odot$ obtained from all mass-complete samples in the COSMOS field at $2 < z < 2.5$. Different markers and colors represent individual special galaxy types – a square, triangle, circle, and hexagon are mergers, SMGs, AGNs, and QGs. Data points are slightly shifted horizontally for clarity. Vertical lines indicate boundaries for each $10^1 M_\odot$ bin.

We also examine the impact of the internal process on galactic properties and galaxy types in this subsection.

3.2.1 Star Formation Activities

We plot the star formation and specific star-formation rates as a function of stellar mass for galaxies at different density contrasts in Figure 8. Overall, all density subsamples follow the so-called star formation main sequence as is reported in the literature (e.g., Daddi et al. 2007; Kashino et al. 2013; Whitaker et al. 2014; Speagle et al. 2014; Tomczak et al. 2016). Meanwhile, the opposite (anti-correlation) is seen in the $sSFR$ vs M_* relation. The median SFR and $sSFR$ are generally independent of the underlying matter density. A possible exception is at $M_* \geq 10^{11} M_\odot$, when the high- Δ subsample ($\Delta_{\text{local}} \geq 4$) shows drops in SFR and $sSFR$. However, a single data point in this bin can preclude a firm conclusion from being reached. We test it in more detail in Section 4.2.1.

3.2.2 Mergers, SMGs, AGNs, and QGs

Figure 9 demonstrates the fraction of each galaxy type as a function of M_* . The notable feature of the plot is a monotonic increase in the fraction with increasing M_* for all galaxy types. Unlike Figure 7, mergers and SMGs are also found across a wide M_* range, with increasing fractions.

The increase of these galaxy types in the mass has also been reported in the literature — mergers (e.g., Bundy et al. 2009), SMGs (e.g., González et al. 2011), AGNs (e.g., general trend Brusa et al. 2009; Tanaka 2012; Pimblet et al. 2013; Lopes et al. 2017, for radio-mode AGN Sabater et al. 2019; Miraghaei 2020), and QGs (e.g., Sobral et

al. 2011; Darvish et al. 2016; Kawinwanichakij et al. 2017; Reeves et al. 2021). Those studies, together with ours in Figure 9 would support the galaxy evolution driven by mass. We will discuss it in more detail in Section 4.2.2.

4 Discussion

4.1 The Impact Of Incomplete Samples To Our Results

Quantifying the impact of a biased sample on the results seen in the mergers, AGNs, SMGs, and QGs is challenging because our spectroscopic sample are only a small fraction of their original catalogs. For instance, our merger and SMG samples are equivalent to only 24 – 30% and 5 – 8% of the original samples.² This small sample size might have enhanced the random chance of selecting galaxies only at lower matter density regions, even in the absence of a physical mechanism. Likewise, the AGNs and QGs within our maps comprise 3 – 4% and 0.8% of the full AGN and QG samples, respectively. The small number statistics could potentially cause a spurious correlation between these object fractions as a function of the density contrast, due to statistical fluctuations. We, therefore, briefly estimate the chance probability of detecting a correlation between the respective population fractions and the density contrast, assuming that Δ_{local} around galaxies is randomly determined. We randomly distributed mock sources with the same sample size as the mass-complete sample across the COSTCO density field and assessed the mock fraction- Δ_{local} relation, i.e., the same plot of Figure 7, by selecting the same number of mock sources with the same total number of original galaxy type shown in Table 1. This test was repeated 1,000 times to evaluate the chance probability.

First, we calculate the probability for finding no mergers and SMGs in the higher density regions due to the small sample sizes. The random probabilities for a spurious absence in high-density regions is found to be less than 2% for all mock merger and SMG samples. For those reasons, we believe that the lack of mergers and SMGs at higher density regions is unlikely to be due to random chance.

Second, we evaluate the probability that the increasing AGN and QG fractions as a function of the density contrast could have occurred from pure chance. We obtain high probabilities of greater than 66% for mock AGNs and QGs to exhibit a correlation with density contrast. This is because in the real data, the number of these objects in each Δ bin becomes smaller with Δ_{local} as seen in Figure 5, whereas the mock AGNs and QGs are ran-

² We only count galaxies whose photo- z are $1.9 \leq z \leq 2.6$ within the respective merger, SMG, AGN, or QG catalogs as original samples.

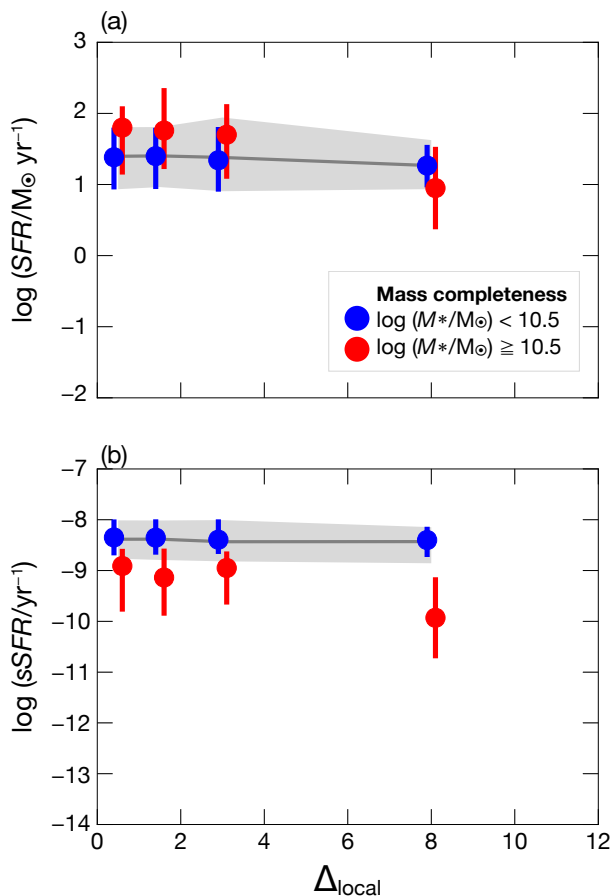


Fig. 10. The median (a) SFR and (b) $sSFR$ of low-/high-mass galaxies as a function of matter overdensity. The Δ_{local} bin size is [1, 1, 2, 8] to increase the sample size in the final bin. The 16th and 84th percentiles are used as errorbars.

domly distributed across the Δ bins. Thus, we cannot rule out the possibility of their random distributions on the density contrast. Although we will conduct the following discussions based on the obtained fractional results, solid conclusions would be made from unbiased, complete data taken by future telescopes (e.g., Giant Magellan Telescope, Thirty Meter Telescope, and Extremely Large Telescope) and instruments.

4.2 The Mechanism For Galaxy Evolution

In Section 3, we studied the relation between galactic properties (i.e., star formation activities and galaxy types) and either underlying matter density contrast or stellar mass. Here we recap those results and discuss the possible mechanisms for galaxy evolution and subsequent star formation quenching.

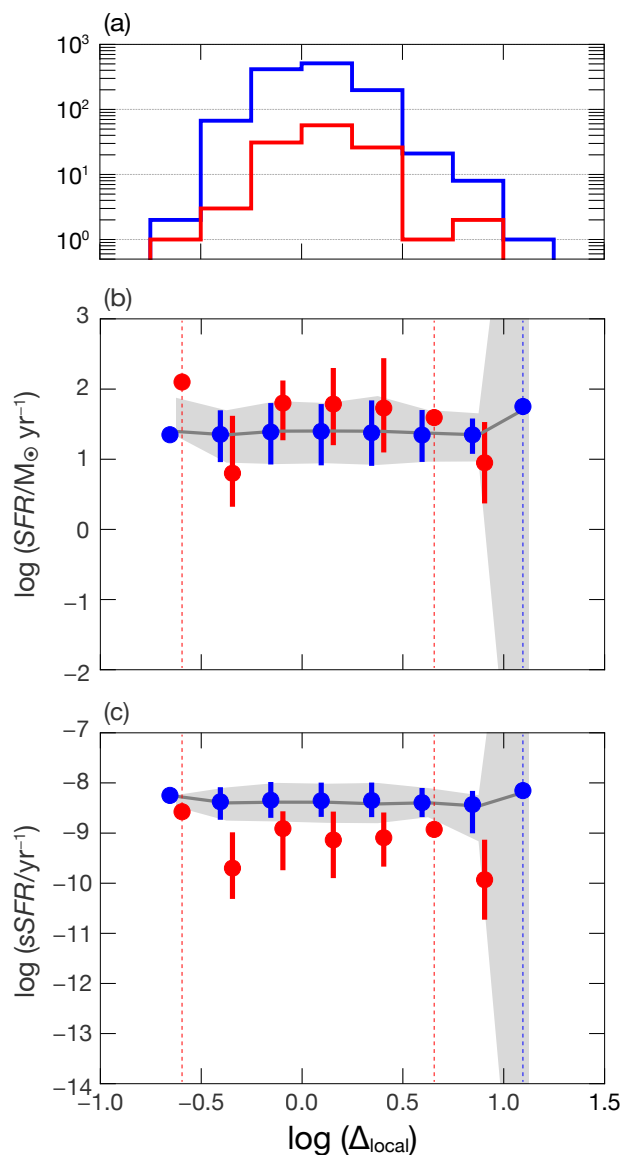


Fig. 11. (a) Number histograms of matter density subsamples in each $\log(\Delta_{\text{local}}) = 0.25$ bin from $\log(\Delta_{\text{local}}) = -1.0$ to 1.5. The median (b) SFR and (c) $sSFR$ of low-/high-mass galaxies as a function of matter overdensity, in log scale. The bin size is $\log(\Delta_{\text{local}}) = 0.25$. The 16th and 84th percentiles are used as errorbars.

4.2.1 The Implication from Star Formation Activities

In Section 3.1.2, we found no dependence of both SFR and $sSFR$ on the density contrast for low-mass galaxies ($M_* < 10^{11} M_{\odot}$). That is also confirmed in the main sequence diagram in Figure 6, in the sense of the lack of dependence among the density subsamples. High-mass galaxies also showed that star formation activities do not depend on the density contrast within the uncertainties. In contrast, their median values demonstrated a decline in high-density regions beyond $\Delta_{\text{local}} = 4 - 6$, as seen in Figures 6 and 8.

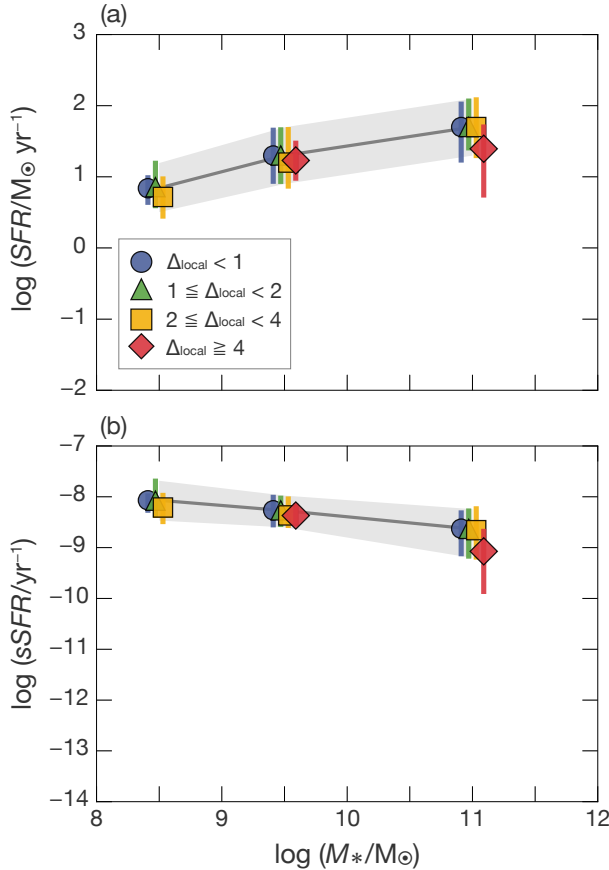


Fig. 12. The median (a) SFR and (b) $sSFR$ as a function of stellar mass, in log scale, for matter density subsamples. The $\log M_*$ bin sizes are [1, 1, 2]. The usage of symbols and lines are the same as Figure 8.

The significance of these declines, however, is low because the median values on SFR and $sSFR$ are from only one sample in the bin showing a decline. We more thoroughly evaluate the significance of the declines in star formation activities for high-mass galaxies in high-density regions by re-binning Δ_{local} and M_* .

We apply the re-binning for Δ_{local} in two ways. The first is to combine all Δ_{local} -bins greater than 4 into one to boost the sample size for high-mass galaxies in high-density regions, as presented in Figure 10. The other way is to evaluate the star formation activities on Δ_{local} in log-scale, as shown in Figure 11. In both cases, SFR and $sSFR$ for high-mass subsamples do not significantly vary on the Δ_{local} within the error, albeit their median values decline by an order of magnitude at the densest bin of $\Delta_{\text{local}} \geq 4$.

For M_* , we re-bin by combining all bins at $M_* \geq 10^{10} M_{\odot}$ into one to increase the sample size for the high- Δ subsample. Figure 12 demonstrates the results. The overall trend is the same as seen in Section 3.2.1 that both SFR and $sSFR$ values are comparable in each M_* bin, regardless of Δ subsamples. Although their median values

for high- Δ subsample show a small drop by about 0.5 dex at $M_* \geq 10^{10} M_{\odot}$, they are still within the error.

To conclude these tests via re-binning, we find comparable in SFR and $sSFR$ within the uncertainties, regardless of stellar mass or Δ of galaxies. In other words, star formation activities in galaxies at $z = 2$ are generally independent of the local matter density but depend on the stellar mass. This implies that the stellar mass of galaxies plays a major role in star formation activities and quenching. This is consistent with some observational studies based on *galaxy* overdensities. According to Darvish et al. (2016), the median SFR s of galaxies at $z > 1$ are almost independent of their overdensities. In addition, they have also found the independence of the median SFR on the overdensity at fixed stellar mass bins for star-forming galaxies out to $z \sim 3$. Chang et al. (2022) have studied green valley galaxies and observed no significant difference in $sSFR$ between the highest and lowest density environments at $1.0 < z < 2.5$.

Despite these results, it is noteworthy that we still identify the decline of the median of SFR and $sSFR$ for high-mass galaxies inside overdense regions in all tests, as seen in Sections 3.1.2 and 3.2.1. A similar dependence of star formation activities on *galaxy* overdensities has been reported in the literature. Chartab et al. (2020) have found the anti-correlation of the SFR with overdensities for their massive samples in $M_* \geq 10^{11} M_{\odot}$ at $z < 3.5$; however they have not detected its significant environmental dependence for their low mass samples ($M_* < 10^{11} M_{\odot}$). Lemaux et al. (2022) have observed a decline of SFR with galaxy overdensities for galaxies in the densest regions at $2.0 < z < 2.7$. If these phenomena hold true, it may suggest the additional environmental effects or other processes working for galaxies satisfying some conditions (i.e., high mass and within overdensities). The ‘‘overconsumption’’ of cold gas could be a viable physical process for such circumstances, which occur only in high-mass galaxies in higher-density regions. The timescale of gas depletion (τ_{dept}) for forming stars is proportional to the ratio of gas mass to SFR ($\tau_{\text{dept}} \propto M_{\text{gas}}/SFR$). Since SFR depends on both stellar mass and redshift, τ_{dept} gets shorter in high-mass galaxies than low-mass ones in the case of the same amount of gas. On the other hand, M_{gas} can be determined by the balance of secular outflows and inflows. Cosmological hydrodynamic simulations by van de Voort et al. (2017) have suggested that the gas accretion rate is suppressed in denser environments, which leads to a shorter gas depletion of galaxies in denser environments. This more significantly affects high-mass galaxies at denser environments and results in the suppression of their star formation on short timescales (see also Balogh et al. 2016; Kawinwanichakij

et al. 2017; Chartab et al. 2020), known as the overconsumption. Our high-mass samples in high-density regions might also suffer from this overconsumption of gas reservoirs and thus show sudden drops in their star formation activity. However, again, we cannot conclude this scenario from our current results due to the significant uncertainties.

4.2.2 The Implication from Merger, SMG, AGN, and QG Fractions

The spectroscopic samples of mergers, SMGs, AGN, and QGs comprise only a small fraction of the main galaxy samples, as discussed in Section 4.1. This brings large uncertainties in our results shown in Section 3.1.3. Nonetheless, it is worth providing some possible scenarios for star formation quenching and environmental dependence based on our results.

A strong dependence on the merger, SMG, AGN, and QG fractions is found on the stellar mass, M_* . All four categories show a positive correlation of their prevalence with M_* (Figure 9). That would be another support that mass is a main driver of galaxy quenching.

By contrast, the density dependence is different between these categories. Galaxies show increasing AGN and QG fractions with their underlying density. A higher QG fraction at higher density regions could be reasonable, given the lower star formation activities of high-mass galaxies seen at $\Delta_{\text{local}} \geq 4 - 6$. The increase of AGN and QG fractions with the density contrast can also be explained by the linear theory prediction and Figure 9. In other words, massive galaxies that have a greater probability of hosting AGNs and/or QGs tend to be located in high-density regions, resulting in a positive correlation with the local density. In contrast, the remaining two types, mergers and SMGs show no clear dependence on the density and are even devoid at higher density regions in $\Delta_{\text{local}} \geq 4$. Those results contradict the scenario predicted by linear theory and Figure 9, in which all these populations become more correlated with M_* and therefore with the density as well.

We discuss some possible causes of the contradiction for no mergers and SMGs within our spec- z samples in higher-density regions. Firstly, that could be simply due to random chance. However, this situation seems to be unlikely, as discussed in Section 4.1. Secondly, it results from the coevolution of galaxies and their surrounding cosmic web. In other words, galaxies fall into higher density regions while changing their properties. If it is the case, galaxies in the transformational phase from star-forming to quiescent, such as mergers, SMGs, and AGNs, could spend this phase in intermediate matter densities. This can also explain the increase of QGs fractions with the density con-

trast, in the sense that galaxies quench their star formation by the time they arrive in higher density regions. A possible conflict of this scenario is the presence of AGNs in higher density regions at $\Delta_{\text{local}} \geq 4$. We may interpret it in terms of different timescales for quenching star formation in galaxies. According to the merger-driven quenching scenario, the merging of two star-forming galaxies leads to a significant circumnuclear starburst. It simultaneously causes the gas inflow to the supermassive black holes and feeds an AGN in the center of the galaxy. The AGN feedback results in the rapid heating and removal of the cold gas and consequently quenching of star-formation within the galaxy (e.g., Sanders & Mirabel 1996; Springel et al. 2005; Springel et al. 2005; Hopkins et al. 2006; Hopkins et al. 2008; Yuan et al. 2010; Alexander & Hickox 2012). Therefore, given this scenario, the AGN phase comes after the dusty star-forming phase, and it occurs just before reaching a quiescent phase. The different timescales after each phase of mergers, SMGs, and AGNs to transform into the QG phase (hereafter, referred to as quenching time) has been suggested in the literature. The quenching time inferred for SMGs — after mergers and subsequent enhanced star formation — has been suggested as a few Gyr, whereas the post-AGN timescale has been inferred to be $\lesssim 1$ Gyr (e.g., Hopkins et al. 2008; Schawinski et al. 2009; Rodríguez Montero et al. 2019). If this is the case with our samples, galaxies may traverse through intermediate matter density regions when they are undergoing the merger and SMGs phases but then migrate to higher density regions while changing their phase to AGNs.

This second situation allows further insight into the process of quenching. The lack of galaxies in the early transforming phase of galaxy evolution at higher densities is reminiscent of “pre-processed” quenching of galaxies in clusters. Zabludoff & Mulchaey (1998) reported that a dominant fraction of elliptical galaxies in clusters may form via mergers in group environments before they accrete into clusters. Subsequent theoretical and observational studies have also claimed that physical mechanisms, such as mergers and ram pressure stripping, operating in intermediate density environments (e.g., groups, filaments, subclusters) are responsible for terminating star formation of galaxies in clusters (e.g., Fujita 2004; De Lucia et al. 2012; Vijayaraghavan & Ricker 2013; Taranu et al. 2014; Pallero et al. 2019). This phenomenon is referred to as pre-processing. Recently, McNab et al. (2021) have found no significant excess of transition galaxies – post-starburst, blue quiescent, and green valley galaxies – of the high-mass regime ($M_* > 10^{10.5} M_\odot$) in clusters at $z \sim 1$. To interpret these findings, they have suggested quenching via pre-processing for high-mass galaxies. Assuming

this is also the case with our samples, galaxies may undergo merger-driven starbursts in regions with a local matter density contrast of $\Delta_{\text{local}} < 4$, corresponding to fields and protocluster outskirts, and terminate their star formation before or during accretion onto high-density regions. Consequently, mergers and SMGs would not possibly be seen in higher-density regions, whereas QGs and AGNs fractions increase with the matter density.

5 Summary

This study demonstrated the dependence of galactic properties, specifically star formation activities (i.e., SFR and $sSFR$) and galaxy types, on the environment and the stellar mass for galaxies at $z = 2$. For the first time, we investigated the environment around galaxies by directly referring to the estimated matter density instead of using a smoothed galaxy overdensity field. The matter density was evaluated from galaxy catalogs and Ly α forest observations by applying numerical reconstruction techniques. Our reconstructed density field allowed us for the first time to study the relationship between galaxies and underdensities at $\Delta_{\text{local}} < 1$ in detail. Using the reconstructed density field, COSTCO, we drew the following conclusions:

1. We found the lack of dependence of star formation activities on the matter density contrast (Δ_{local}) over uncertainties for both low-mass ($M_{\star} < 10^{10.5} M_{\odot}$) and high-mass galaxies ($M_{\star} \geq 10^{10.5} M_{\odot}$). Nonetheless, it is still notable that we detect a consistent pattern of decreased star formation activities for high-mass galaxies in higher density contrast at $\Delta_{\text{local}} \geq 4$ from all analyses, including rebinning, even though it is just from the median value. However, that statistical significance is low due to the large uncertainties. A larger sample with future surveys will provide solid conclusions with high significance.
2. We examined the fraction of mergers, SMGs, AGNs, and QGs relative to the density contrast. Although our results in the above special galaxy types are still tentative with large uncertainties, we obtained the following trends. For mergers and SMGs, we see no clear dependence on the density contrast but find a lack of those types at higher density regions of $\Delta_{\text{local}} \geq 4$. The probability of accidental occurrence of the lack of those samples at higher density regions was found to be low. Those results could indicate that mergers and SMGs tend to avoid higher-density regions. In contrast, AGN and QG fractions were found to increase with increasing the density contrast. Considering all results from merg-

ers, SMGs, AGNs, and QGs, we may infer a scenario in which galaxies evolve by transforming their properties while they migrate through the various density regimes of the cosmic web. In addition, the lack of mergers and SMGs may also imply the pre-processing of galaxy quenching.

3. We also studied the relation between galactic properties and the stellar mass (M_{\star}). The SFR and $sSFR$ for a fixed M_{\star} bin were nearly the same across all Δ subsamples within their uncertainties. A possible exception was detected for the high-mass regime at $M_{\star} \geq 10^{11} M_{\odot}$ of the high- Δ_{local} subsample ($\Delta_{\text{local}} \geq 4$), though its significance is still low. In terms of mergers, SMGs, AGN, and QGs, we found a significant correlation between their fractions and M_{\star} for all galaxy types, unlike the density dependence. This could be another hint of mass-driven galaxy evolution.

As we already argued, mass quenching must be the main driver of our galaxies at $z = 2$. Nonetheless, environmental quenching cannot be completely ruled out. Although statistical significance is low due to a single data point, we still tentatively detected the sudden drop in star formation activities for high-mass galaxies in higher-density regions. We also tentatively found the change in the fraction of mergers, SMGs, AGNs, and QG with the local matter density. If those detections were real, they may indicate the environmental quenching described well by “overconsumption” and “pre-processing” models. Our galaxies might undergo mergers and subsequent starbursts at the intermediate density while traveling to the high density and gradually quench their star formation, known as pre-processing. Besides, high-mass galaxies in higher-density environments, $\Delta_{\text{local}} \geq 4 - 6$ in case of our results, could have additional effects on the environment, called overconsumption, and accelerate their quenching. More solid conclusions would be drawn from the complete galaxy samples in future surveys, such as by the Prime Focus Spectrograph (PFS; Sugai et al. 2015) on the Subaru telescope. This next-generation facility should also enable more detailed studies involving the anisotropic cosmic web, including possible constraints on high-redshift galaxy intrinsic alignments to the cosmic web (Krolewski et al. 2017; Zhang et al. 2022).

Acknowledgments

We are grateful to Dr. Andrea Silva for kindly sharing the merger catalogs and Drs. Louise Edwards, Nima Chartab, Andrew B. Newman, and Mahdi Qezlou for helpful discussions. We also thank the attendees of the 2023 KITP Cosmic

Web Conference, *The Co-evolution of the Cosmic Web and Galaxies across Cosmic Time*, including Drs. Chris Byrohl, Farhanul Hasan, Clotilde Laigle, Jounghun Lee, Hyunbae Park, and Hyunmi Song. We also appreciate an anonymous referee for their valuable comments on improving our manuscript. R.M. acknowledges a Japan Society for the Promotion of Science (JSPS) Fellowship at Japan. This work is supported by the JSPS KAKENHI grant Nos. JP18J40088 and JP21H04490 (R.M.), JP18H058681418, JP19K14755 (K.G.L.), and JP21K13911 (M.A.). MA was supported by Simons Collaboration on “Learning the Universe”. Kavli IPMU was established by World Premier International Research Center Initiative (WPI), MEXT, Japan. Some of the data presented herein were obtained at the W.M. Keck Observatory, which is operated as a scientific partnership among the California Institute of Technology, the University of California and the National Aeronautics and Space Administration (NASA). The Observatory was made possible by the generous financial support of the W.M. Keck Foundation. The authors also wish to recognize and acknowledge the very significant cultural role and reverence that the summit of Maunakea has always had within the indigenous Hawai’ian community.

Appendix 1 Tests for the Dependence on Stellar Mass Threshold

We test the impact on the stellar mass threshold for the results on high-mass galaxies by changing it as $\log M_*/M_\odot = 10.50, 10.00, 9.76$. Note that the number of high-mass samples in these cases is (121, 417, 672) for $\log M_*/M_\odot = 10.50, 10.00, 9.76$, in which the sample size for $\log M_*/M_\odot = 9.76$ is half of the all of our sample. We use the same bin size as Figure 10 to verify the trend. The results on star formation activities on Δ_{local} for high-mass subsample are shown in Figure 13. Both subsamples for $\log M_*/M_\odot = 10.00$ and 9.76 show consistency on SFR and $sSFR$ with each other. In addition, there is no significant dependence on Δ_{local} beyond the uncertainties. Nonetheless, their median values show a slight decline, as we saw in the case of high-mass galaxies with the threshold of $\log M_*/M_\odot = 10.50$. Their star formation activities decrease by $0.30 - 0.40$ and $0.16 - 0.22$ dex, for $\log M_*/M_\odot = 10.00$ and 9.76 subsamples, respectively.

These tests reveal a qualitatively similar trend for high-mass galaxies in the relationship between star formation activities and Δ_{local} , regardless of the M_* thresholds, at least those utilized in the test. We find no significant dependence of star formation activities on Δ_{local} beyond uncertainties. Nonetheless, it would be interesting that all subsamples detect a decline of their median values at $\Delta_{\text{local}} \geq 4.0$. Given the extent of decrease for 10.00 and 9.76 thresholds being smaller compared to the subsample with a 10.50 threshold, using a 10.50 threshold could help to confirm a trend clearly if that presents in the star for-

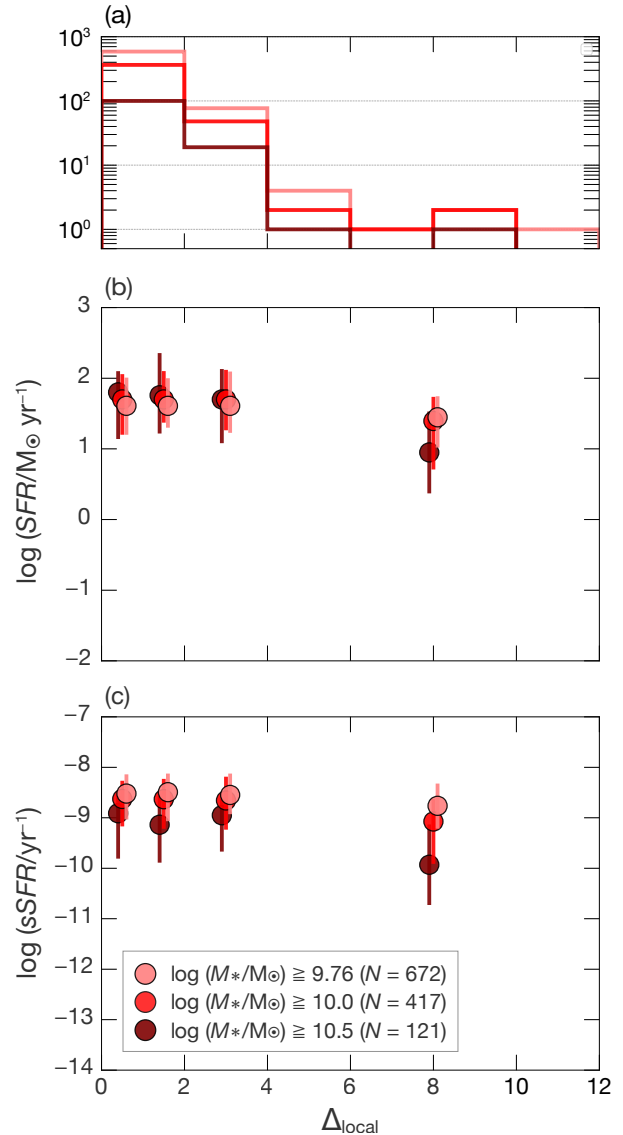


Fig. 13. (a) Number histograms of stellar mass subsamples in each $\Delta_{\text{local}} = 2$ bin. The median (b) SFR and (c) $sSFR$ of high-mass galaxies as a function of matter overdensity. The Δ_{local} bin size is [1, 1, 2, 8] to increase the sample size in each M_* bin. The 16th and 84th percentiles are used as errorbars. Different colors represent different stellar mass thresholds for mass subsamples.

mation activities and Δ_{local} relations.

Appendix 2 Test for the Variation on Δ_{local} Criteria

In Figure 14, we test the impact on the matter density threshold for the results on high- Δ_{local} subsample. We used the threshold for the high- Δ_{local} subsample of $\Delta_{\text{local}} \geq 2.0, 2.5, 3.0, 3.5, 4.0$ whose sample sizes are (172, 71, 41, 23, 18). All subsamples are consistent with the entire median, as shown by the grey line within the uncertainties. The

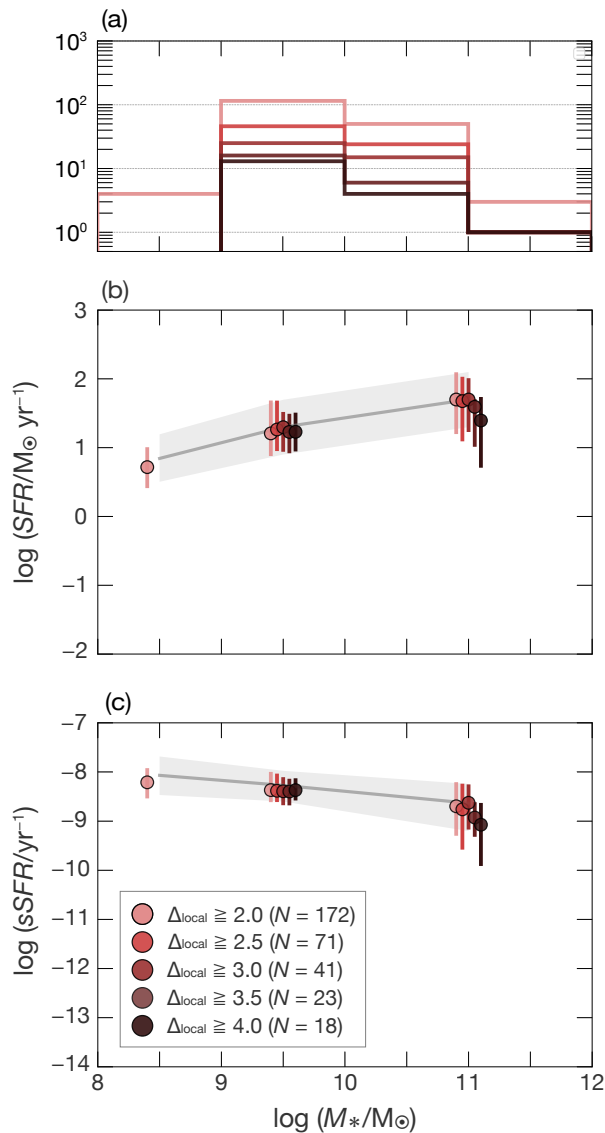


Fig. 14. (a) Number histograms of matter density subsamples in each $M_* = 10^1 M_\odot$ bin from $M_* = 10^8$ to $10^{12} M_\odot$. The median (b) SFR and (c) $sSFR$ to M_* in $\log M_*$ bin sizes of [1, 1, 2]. The error bars indicate the percentiles 16th and 84th of SFR and $sSFR$. A gray line and shades are the medians and 68 percentiles of SFR and $sSFR$ of the entire mass-completeness sample. Data points are slightly shifted horizontally for clarity. Different colors represent different Δ thresholds for matter density subsamples.

possible decline of medians is confirmed only in $\Delta_{\text{local}} \geq 3.5$ and 4.0 subsamples, which are 0.1–0.3 dex and 0.3–0.4 dex in SFR and $sSFR$ to the entire median.

These tests show that the matter density threshold could influence the results on the high- Δ_{local} subsample. The decline of star formation activities in high-mass galaxies in the highest density region, as commonly seen in the main text, though its statistical significance is low, is only observed when we apply the threshold $\Delta_{\text{local}} \geq 3.5$. If our

results reflect a true relation of galaxy properties on the matter density contrast in the universe, the regions with $\Delta_{\text{local}} \geq 3.5$ might be special at $z \sim 2$ as causing the environmental quenching. Hence, it might be intriguing to study such regions in more detail in the context of galaxy evolution together with the cosmic web utilizing upcoming galaxy survey data.

References

- Alexander D. M. & Hickox R. C., 2012, *Nature*, 56, 93
 Álvarez Crespo, N., et al. 2021, *A&A*, 646, 174
 Ando M., Shimasaku K. & Momose R. 2020, *MNRAS*, 496, 3169
 Ata M., et al. 2022, *Nature*, 6, 857
 Ata M., et al. 2021, *MNRAS*, 500, 3194
 Baldry I. K., et al. 2004, *ApJ*, 600, 681
 Balogh M. L., et al. 2016, *MNRAS*, 456, 4364
 Balogh M. L., Navarro J. F. & Morris S. L. 2000, *ApJ*, 540, 113
 Bekki K., 2014, *MNRAS*, 438, 444
 Behroozi P., et al., 2019, *MNRAS*, 488, 3143
 Behroozi P. S., Wechsler R. H., & Conroy C., 2013, *ApJ*, 770, 57
 Blanton M. R. & Moustakas J. 2009, *ARA&A*, 47, 159
 Blanton M. R., et al. 2005, *ApJ*, 629, 143
 Blanton M. R., et al. 2003, *ApJ*, 594, 186
 Boselli A., Fossati M. & Sun M. 2022, *A&AR*, 30, 3
 Brammer G. B., et al. 2009, *ApJL*, 706, L173
 Brisbin D., et al. 2017, *A&A*, 608, 15
 Brusa M., et al. 2007, *A&A*, 507, 1277
 Bundy K., et al. 2009, *ApJ*, 697, 1369
 Capak E., et al. 2007, *ApJS*, 172, 99
 Casey C. M., 2016, *ApJ*, 824, 36
 Champagne J. B., et al. 2021, *ApJ*, 913, 110
 Chang W., et al. 2022, *ApJ*, 936, 47
 Chapman S. C., et al. 2009, *ApJ*, 691, 560
 Chartab N., et al. 2020, *ApJ*, 890, 7
 Chuter R. W., et al. 2011, *MNRAS*, 413, 1678
 Cowley M. J., et al. 2016, *MNRAS*, 457, 629
 Croton D. J., et al. 2006, *MNRAS*, 365, 11
 Daddi E., et al. 2007, *ApJ*, 670, 156
 Dalla Vecchia C. & Schaye J. 2008, *MNRAS*, 387, 1431
 Darvish B., et al. 2016, *ApJ*, 825, 113
 De Lucia G., et al. 2012, *MNRAS*, 423, 1277
 Dekel A. & Silk J. 1986, *ApJ*, 303, 39
 Delahaye A. G., et al. 2017, *ApJ*, 843, 126
 Delvecchio I., et al. 2017, *A&A*, 602, 3
 Digby-North J. A., et al. 2010, *MNRAS*, 407, 846
 Dong C., et al. 2023, *ApJL*, 945, L28
 Fabian A. C., 2012, *ARA&A*, 50, 455
 Fang J. J., et al. 2013, *ApJ*, 776, 63
 Fossati M., et al. 2017, *ApJ*, 835, 153
 Fujita Y., 2004, *PASJ*, 56, 29
 González J. E., et al. 2011, *MNRAS*, 413, 749
 Gunn J. E. & Gott J. R. III 1972, *ApJ*, 176, 1
 Guo Y., et al. 2017, *ApJL*, 841, L22
 Hashimoto T., et al. 2013, *ApJ*, 765, 70

- Hickox R. C., et al. 2012, MNRAS, 421, 284
Hine N. K., et al. 2016, MNRAS, 455, 2363
Horowitz B., et al. 2019, ApJ, 887, 61
Horowitz B., et al. 2021, ApJ, 906, 110
Hopkins P. F., et al. 2008, ApJS, 175, 356
Hopkins P. F., et al. 2006, ApJ, 652, 864
Huang Y., et al. 2022, ApJ, 941, 134
Ilbert O., et al. 2013, A&A, 556, 55
Ilbert O., et al. 2006, A&A, 457, 841
Ito K., et al. 2022, ApJ, 929, 53
Ito K., et al. 2021, ApJ, 916, 35
Jasche J. & Wandelt B. D. 2013, MNRAS, 432, 894
Ji Z., et al. 2018, ApJ, 862, 135
Jones S. F., et al. 2017, MNRAS, 469, 4565
Kashino D., et al. 2013, ApJL, 777, L8
Kauffmann G., et al. 2004, MNRAS, 353, 713
Kauffmann G., et al. 2003, MNRAS, 341, 33
Kawata D. & Mulchaey J. S. 2008, ApJL, 672, L103
Kawinwanichakij L., et al. 2017, ApJ, 847, 134
Kitaura F.-S., et al. 2021, MNRAS, 502, 3456
Kriek M., et al. 2015, ApJS, 218, 15
Krishnan C., et al. 2017, MNRAS, 470, 2170
Krolewski A., et al. 2017, ApJ, 837, 31
Krolewski A., et al. 2018, ApJ, 861, 60
Larson R. B., Tinsley B. M. & Caldwell C. N. 1980, ApJ, 237, 692
Le Fèvre O., et al. 2015, A&A, 576, 79
Lee K.-G., et al. 2018, ApJS, 237, 31
Lee K.-G., et al. 2016, ApJ, 817, 160
Lee K.-G., et al. 2014, ApJL, 795, L12
Lehmer B. D., et al. 2009, ApJ, 691, 687
Lemaux B. C., et al. 2022, A&A, 662, 33
Liang Y., et al. 2021, ApJ, 907, 3
Lilly S. J., et al. 2007, ApJS, 172, 70
Lin L., et al. 2016, ApJ, 817, 97
Lopes P. A. A., Ribeiro A. L. B. & Rembold S. B. 2017, MNRAS, 472, 409
Lotz J. M., et al. 2013, ApJ, 773, 154
Macuga M., et al. 2019, ApJ, 874, 54
Man Z., et al. 2019, MNRAS, 488, 89
Martini P., et al. 2013, ApJ, 768, 1
McCarthy I. G., et al. 2008, MNRAS, 383, 593
McNab K., et al. 2021, MNRAS, 508, 157
Michałowski M., et al. 2017, MNRAS, 469, 492
Miller T. B., et al. 2015, MNRAS, 452, 878
Miller T. B., et al. 2003, ApJ, 597, 142
Miraghaei H., 2020, AJ, 160, 227
Momose R., et al. 2021b, ApJL, 912, L24
Momose R., et al. 2021a, ApJ, 909, 117
Moore B., Lake G. & Katz N. 1998, ApJ, 495, 139
Moore B., et al. 1996, Nature, 379, 613
Moster B. P., Naab T., & White S. D. M. 2013, MNRAS, 428, 3121
Muzzin A., et al. 2012, ApJ, 746, 188
Nakajima K., et al. 2013, ApJ, 769, 3
Nanayakkara T., et al. 2016, ApJ, 828, 21
Nantais J. B., et al. 2016, A&A, 592, 161
Overzier R. A., et al. 2008, ApJ, 673, 143
Pallero D., et al. 2019, MNRAS, 488, 847
Peng Y., et al. 2012, ApJ, 757, 4
Peng Y., et al. 2010, ApJ, 721, 193
Pimblet K. A., et al. 2013, MNRAS, 429, 1827
Polletta M., et al. 2021, A&A, 654, 121
Quadri R. F., et al. 2012, ApJ, 744, 88
Reeves A. M. M., et al. 2021, MNRAS, 506, 3364
Rodríguez Montero F., et al. 2019, MNRAS, 490, 2139
Sabater J., et al. 2019, A&A, 622, 17
Sanders D. B. & Mirabel I. F. 1996, ARA&A, 34, 749
Schawinski K., et al. 2009, ApJ, 690, 1672
Scoville N., et al. 2007, ApJS, 172, 1
Shah E. A., et al. 2020, ApJ, 904, 107
Shi K., et al. 2019, ApJS, 879, 9
Shibuya T., et al. 2014, ApJ, 788, 74
Shimakawa R., et al. 2017, MNRAS, 468, 21
Silva A., et al. 2018, ApJ, 868, 46
Silverman J. D., et al. 2009, ApJ, 695, 171
Smith K., et al. 2016, ApJ, 833, 109
Smith R., et al. 2015, MNRAS, 454, 2502
Smith R., et al. 2013, MNRAS, 429, 1066
Smith R., Davies J. I. & Nelson A. H. 2010, MNRAS, 405, 1723
Smolčić V., et al. 2012, A&A, 548, 4
Sobral D., et al. 2011, MNRAS, 411, 675
Speagle J. S., et al. 2014, ApJS, 214, 15
Springel V., Di Matteo T., & Hernquist L. 2005, ApJL, 620, L79
Springel V., Di Matteo T., & Hernquist L. 2005, MNRAS, 361, 776
Straatman C. M. S., et al. 2016, ApJ, 830, 51
Strateva I., et al. 2001, AJ, 122, 1861
Sugai H., et al. 2015, Journal of Astronomical Telescopes, Instruments, and Systems, 1, 5001
Tanaka M., 2012, PASJ, 64, 37
Taranu D. S., et al. 2014, MNRAS, 440, 1934
Tomczak A. R., et al. 2016, ApJ, 817, 118
Toomre A. & Toomre J. 1972, ApJ, 178, 623
Toshikawa J., et al. 2016, ApJ, 826, 114
Tran K.-V. H., et al. 2010, ApJL, 719, L126
Umehata H., et al. 2015, ApJL, 815, L8
van de Voort F., et al. 2017, MNRAS, 466, 3460
Venemans B. P., et al. 2007, A&A, 461, 823
Vijayaraghavan R., & Ricker P. M. 2013, MNRAS, 435, 2713
von der Linden A., et al. 2010, MNRAS, 404, 1231
Watson C., et al. 2019, ApJ, 874, 63
Weaver J. R., et al. 2023, A&A, 677, 184
Weaver J. R., et al. 2022, ApJS, 258, 30
Wetzell A. R., Tinker J. L., & Conroy C. 2012, MNRAS, 424, 232
Whitaker K. E., et al. 2014, ApJ, 795, 104
Wilkinson A., et al. 2017, MNRAS, 464, 1380
Williams R. J., et al. 2009, ApJ, 691, 1879
Willmer C. N. A., et al. 2006, ApJ, 647, 853
Wyder T. K., et al. 2007, ApJS, 173, 293
Yuan T.-T., Kewley L. J., & Sanders D. B. 2010, ApJ, 709, 884
Zabludoff A. I., & Mulchaey J. S. 1998, ApJ, 496, 39

Zavala J. A, et al. 2019, *ApJ*, 887, 183

Zeballos M., et al. 2018, *MNRAS*, 479, 4577

Zhang B., et al. 2022, *arXiv:2211.09331*